



Long- and Short-Term Evolutions of Magnetic Field Fluctuations in High-Speed Streams

Gilbert Pi^{1,2} · Alexander Pitňa¹ · Zdenek Němeček¹ ·
Jana Šafránková¹ · Jih-Hong Shue² · Ya-Hui Yang²

Received: 21 October 2019 / Accepted: 1 June 2020
© Springer Nature B.V. 2020

Abstract High-speed streams (HSSs) are believed to be only slightly affected by different interactions on their path from the Sun to Earth and thus the analysis of their observations can provide information on the structure and temporal variations of the magnetic field and plasma parameters at the source region. We have chosen three coronal holes supplying 14 HSSs recorded by Wind in 2008. For each HSS, we have calculated the average magnetic field and plasma parameters as well as power spectral densities (PSDs) of magnetic field fluctuations in the MHD and kinetic ranges to investigate their long- and short-term variations. We suggest that long-term variations are connected with a time evolution of the source region on the time scale of solar rotations. On the other hand, the short-term variations would reflect a longitudinal structure of the coronal hole. Our study reveals that coronal holes are very stable source of HSSs and their temporal evolution on short- and long-time scales is negligible. This is true for the average parameters as well as for the fluctuation power and PSDs. Observed correlations between bulk and/or thermal velocity and PSD parameters are consistent with already published results. We suggest that they do not originate in the source region but they can be mostly attributed to interaction with the ambient slow wind that affects even the HSS core.

1. Introduction

The solar wind brings the fluctuating solar magnetic field into interplanetary space. During propagation, the turbulent energy cascades from larger to smaller scales and forms a typical power-law frequency spectrum. The power spectral density (PSD) profile of interplanetary

This article belongs to the Topical Collection:
Solar Wind at the Dawn of the Parker Solar Probe and Solar Orbiter Era
Guest Editors: Giovanni Lapenta and Andrei Zhukov

✉ J.-H. Shue
jhshue@jupiter.ss.ncu.edu.tw

¹ Faculty of Mathematics and Physics, Charles University, Prague, Czech Republic

² Institute of Space Science, National Central University, Jhongli City, Taoyuan County 32001, Taiwan

magnetic field (IMF) fluctuations can provide abundant information on the energy cascade and how this is related to wave–particle interactions with the plasma.

At inertial scales, the magnetic field fluctuations pose a Kolmogorov-like spectrum with a slope of $-5/3$. When reaching the proton kinetic scales, the magnetic spectra steepen with a spectral index varying between -4 and -2 at sub-ion scales (Leamon et al., 1998; Smith et al., 2006; Sahraoui et al., 2010; Bruno and Carbone, 2013) but typically close to ~ -2.8 in the range between the ion and electron scales (Alexandrova, 2008; Alexandrova et al., 2009, 2012; Sahraoui et al., 2013; Kiyani, Osman, and Chapman, 2015; Kiyani et al., 2013, Koval and Szabo, 2013). Leamon et al. (1998) have shown that the spectral indices of magnetic field fluctuations are correlated with the proton temperature; the hotter plasma is accompanied by a steeper power-law in the kinetic range.

As discussed by many authors, the power spectra exhibit different characteristics in fast and slow solar wind (e.g., Borovsky, 2012; Bruno and Telloni, 2015) because the flows differ not only in average values of the magnetic field and plasma parameters, but also in the type of fluctuations they transport. The fast wind is characterized by large-amplitude, incompressible fluctuations, mainly of the Alfvénic nature (e.g., Matteini et al., 2014). The slow wind, on the other hand, is generally populated by less Alfvénic fluctuations with smaller amplitudes, predominantly of compressive nature (Bruno and Telloni, 2015; Bruno et al., 2017).

Based on the magnetic field data observed by the ACE spacecraft, Smith et al. (2006) considered the spectral properties of fluctuations at frequencies ≥ 0.3 Hz in the spacecraft frame, and demonstrated that the power-law index in the dissipation range depends on the rate at which energy cascades through the inertial range. They included magnetic cloud observations and the open magnetic field intervals and found that spectral indices in the inertial range are between $-3/2$ to $-5/3$. Spectral indices were more variable in the kinetic range (\sim between -1 and -4), similar to those reported by Leamon et al. (1998) and Sahraoui et al. (2010), with the mean values of -2.61 and -2.01 in open magnetic field regions and clouds, respectively. Turbulence in the kinetic range was studied by Pitňa et al. (2019) and they found that the spectral slope roughly follows the prediction for kinetic Alfvén waves on average but the slopes determined from Wind magnetic field measurements range from -1.5 to -3.5 . The authors argued that the flat spectra are contaminated by the instrumental noise and/or aliasing, and only slopes steeper than -2 are likely to be physical.

Using ten years of ACE magnetic field observations at the L1 point, Borovsky (2012) carried out an extensive study of magnetic field fluctuations in the frequency range of 4.3×10^{-4} to 1.9×10^{-3} Hz for various types of solar-wind plasma passing the spacecraft: i.e., the slow wind, compressed slow wind, compressed fast wind, coronal-hole fast wind, rarefied coronal-hole wind, etc. The spectral index of magnetic field fluctuations varies with solar-wind type, being close to $-5/3$ in the slow wind (< 450 km s $^{-1}$) but -1.54 in the fast wind. There was a large spread of indices from -2.5 to -0.5 , and, moreover, the slope of the magnetic field spectrum increases with plasma density, whereas the fluctuation amplitude increases with solar-wind speed. Using the Zhao, Zurbuchen, and Fisk (2009) scheme, the author also identified the streams emanating from coronal holes (CHs) and found a spectral index of -1.63 for these events. From this complex analysis, it was concluded that the systematic differences in the spectral indices between fast and slow winds are a consequence of differences between coronal-hole and non-coronal-hole plasma.

Bruno, Trenchi, and Telloni (2014) performed an analysis of HSSs interacting with slow wind regions. At proton scales, the spectral slope exhibits a large variability between -3.75 and -1.75 . There was a tendency for the spectral slope to be steeper within the trailing edge of the stream where the speed is higher and to be flatter within the subsequent slower

wind, undergoing a gradual transition between these two states. The spectral index seems to correlate strongly on the power associated with the fluctuations within the inertial range; higher power is associated with a steeper slope. Subsequently, Bruno et al. (2017) focused on co-rotating HSSs coming from the equatorial extension of polar CHs. The HSSs originated in CH areas are characterized by a stream interface, a fast wind region that is followed by a slower refraction region formed at the trailing edge of the stream. A spectral analysis within HSSs showed that the power level of magnetic fluctuations within the inertial range largely decreases from the faster into slower wind. Spectra exhibited the typical Kolmogorov scaling (e.g., Bruno and Carbone, 2013), with a break around the scale of $\lambda_i \cong \rho_i \cong V/(2\pi f_{ci})$, where λ_i is the ion inertial length, ρ_i is the ion Larmor radius, f_{ci} is the ion cyclotron frequency, and V is the solar-wind speed. At proton scales, the spectral index became steeper towards a value around -2.7 .

The CHs are large-scale structures in the solar corona primarily on open magnetic field lines and they are the major source of the high-speed solar wind. Heinemann et al. (2018a) found a strong linear correlation between the magnetic properties (e.g. signed/unsigned magnetic field strength) and the area of the CH. Heinemann et al. (2018b) discussed how different evolutionary states of the CH, as observed in the solar atmosphere (changes in EUV intensity and area), affect the properties of associated HSSs observed at 1 AU. They defined three development phases: (i) growing, (ii) maximum, and (iii) decaying phase and found that the three phases are related to different ranges of solar-wind speeds: 460–600 km s⁻¹ for the growing phase, 600–720 km s⁻¹ for the maximum phase, and a more irregular behavior connected to speeds of 350–550 km s⁻¹ for the decaying phase.

As can be seen from this short overview, the power and spectral indices of fluctuations can vary over a wide range, especially in the fast solar wind. However, it is not clear whether this variability characterizes the source region or it originates during solar-wind transit to an observer. Thus, we address the magnetic field fluctuations in the HSSs associated with identified CHs. We use the wavelet technique to investigate long- and short-term evolutions of the power and slopes of PSDs, and their relation to solar-wind parameters in both inertial and kinetic ranges. The long-term evolution means the changes of HSSs emanating from the same CH and observed over consecutive solar rotations. On the other hand, short-term profiles represent the variations of PSDs at different sub-intervals within a particular HSS. The methodology of event selection and PSD calculations are described in Section 2 and the results are presented in Section 3. The discussion can be found in Section 4 and Section 5 summarizes our conclusions.

2. Data Analysis

Figure 1 presents a stackplot of solar-wind speed as a function of time through Carrington rotation (CR) number, over the years 2008–2009 (i.e., Carrington rotations 2065–2091). We have intentionally chosen solar minimum because the observations of HSSs in the equatorial plane are less frequent and particular HSSs can be easily associated with the source region on the solar surface. We have highlighted three clusters of the daily averaged solar-wind speed greater than 600 km s⁻¹ by white rectangles, labeled CH1, CH2, and CH3. Each of these periods is checked against the solar images from the solar monitor website (www.solarmonitor.org; more information can be found in Gallagher, Moon, and Wang, 2002) to confirm that each HSS reasonably corresponds to an identifiable CH. This website provides a catalog of the daily identifications of CHs based on the CHARM algorithm

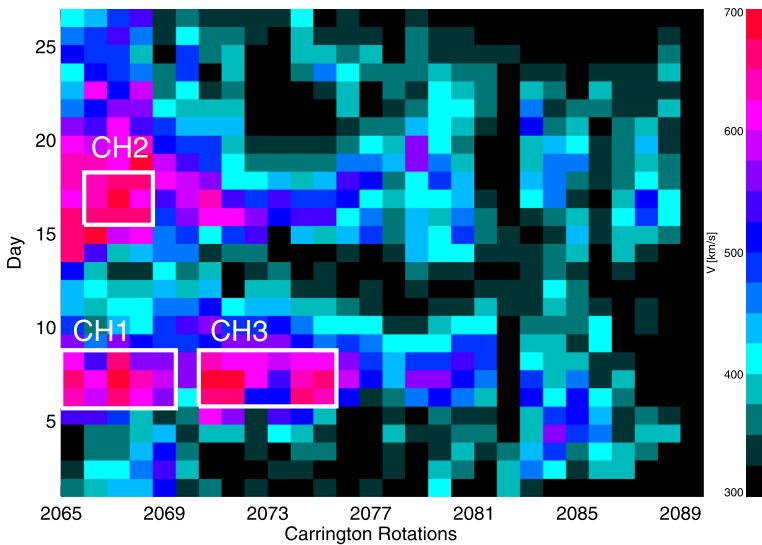


Figure 1 A map of the solar wind bulk speed for the CRs of 2065–2091. The X-axis is for CR numbers of and the Y-axis is for days within a CR. The colors show the daily averaged solar wind bulk speed. The white rectangles show three CHs selected for investigations.

(Krista and Gallagher, 2009). Briefly, full-disk solar EUV images are processed as projection maps, the bimodal distribution of flux intensity in the detected regions is used to identify the different regions, and finally, low intensity regions are classified as a CH. According to the CH images, our three groups of periodic HSSs can be unambiguously associated with three long-lasting CHs in the catalog. We have chosen encounters with 14 HSSs that originated from these three CHs during 2008 for the long-term part of the study. For each HSS we defined start and end times and the details related to the source CH; an overview of these characteristics is listed in Table 1. As can be seen in Figure 1, we did not include the fast wind observations surrounding the white rectangle bounded by 16th and 19th days of CRs 2066–2068 because we were not able to associate them with any CH.

PSDs are computed from the high-resolution magnetic field data obtained by the Magnetic Field Investigation (MFI) instrument onboard the Wind spacecraft, which provides the IMF vector with a cadence of 0.092 s (Lepping et al., 1995; Koval and Szabo, 2013). The plasma properties of HSSs are determined using the data recorded by the Wind/SWE instrument (Ogilvie et al., 1995). SWE provides the anisotropy analysis of the plasma parameters with a 92-second resolution (Kasper et al., 2006); we used only the data with a quality flag 10 that 10=SW parameters OK, denoted in the data description at CDAWeb (<https://cdaweb.gsfc.nasa.gov/>). Figure 2 shows the proton bulk speed, density, temperature and IMF magnitude and components in GSE (Geocentric Solar Ecliptic) coordinates observed during one Example (06/01/2008–09/01/2008) of selected events. The structure of the stream interaction region is rather complicated; it is composed of a compressed leading edge, an unperturbed main body, and an extended trailing region characterized by the gradual velocity decrease. We visually identified the boundaries of these three regions based on the proton speed and density profiles and marked them by the vertical dashed lines in the figure. For removing the effect on compression, we skipped the compressed and rarefied regions and used only the main body of a particular HSS. Since the durations of selected parts of individual HSSs are highly variable, as noted in the introduction, we divided the

Table 1 List of HSS events and the related CHs

HSS No.	Selected period			Related CH [observation date and center location]
	Start time [yyyy/mm/dd hh:mm:ss]	End time [yyyy/mm/dd hh:mm:ss]	Duration [hrs]	
1	2008/01/06 06:25:42	2008/01/08 23:56:19	65.5	CH1 (2008/01/04, N00W05)
2	2008/02/02 10:17:08	2008/02/04 10:05:43	47.8	CH1 (2008/01/31, N29W08)
3	2008/02/11 13:17:08	2008/02/17 05:16:11	136.0	CH2 (2008/02/09, S31E23)
4	2008/02/29 14:34:17	2008/03/02 09:32:56	43.0	CH1 (image missing)
5	2008/03/09 21:51:25	2008/03/15 19:16:26	141.4	CH2 (2008/03/07, S44E32)
6	2008/03/28 06:51:25	2008/03/29 09:09:05	26.3	CH1 (2008/03/25, N10E29)
7	2008/04/06 07:17:08	2008/04/10 21:57:02	110.7	CH2 (2008/04/03, S38E23)
8	2008/04/24 10:17:08	2008/04/25 15:56:01	29.6	CH1 (2008/04/21, N11E21)
9	2008/07/12 17:34:17	2008/07/16 08:25:37	86.9	CH3 (2008/07/11, N09W04)
10	2008/08/10 04:17:08	2008/08/11 17:15:29	37.0	CH3 (2008/08/07, S01E02)
11	2008/09/07 07:42:51	2008/09/09 07:17:08	47.6	CH3 (2008/09/03, S07W00)
12	2008/10/02 12:51:25	2008/10/05 03:09:58	62.3	CH3 (2008/09/29, S04E04)
13	2008/10/30 10:17:08	2008/10/31 05/28/17	19.2	CH3 (2008/10/27, S06W05)
14	2008/11/26 21:25:42	2008/11/27 20:34:17	23.1	CH3 (2008/11/23, N26W04)

HSS profiles into subintervals of length 6.7 hours (218 magnetic field vectors) for each HSS in order to facilitate the spectral analysis. The subintervals are distinguished by the vertical dotted lines in Figure 2. This procedure was performed for all 14 HSS encounters, resulting in 170 subintervals suitable for the analysis.

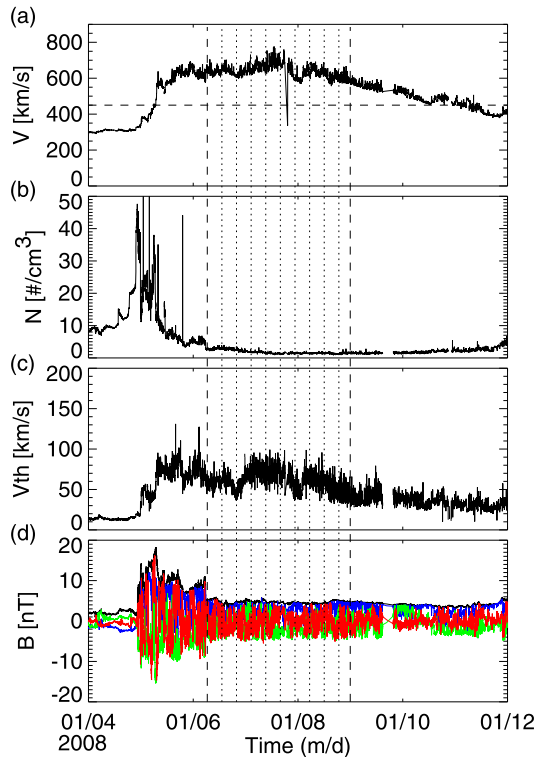
3. Results

The study addresses two main topics: i) evolutions and longitudinal profiles of the average magnetic field and plasma parameters within the HSS core, and ii) the fluctuation properties of CH-related HSSs.

3.1. Evolution of Average Parameters Within HSSs

Figure 3 presents the time evolution of solar-wind and magnetic field parameters and their uncertainties in all 14 HSS encounters associated with three CHs. Each point represents a

Figure 2 Wind observations of the HSS on 4–12 January 2008. From top to bottom: (a) the solar wind bulk speed, (b) density, (c) thermal speed, and (d) magnitude and three components of the magnetic field in GSE coordinates (blue for B_x , green for B_y , and red for B_z). The vertical dashed lines represent the start and end of the chosen CH interval and dotted lines separate individual subintervals.

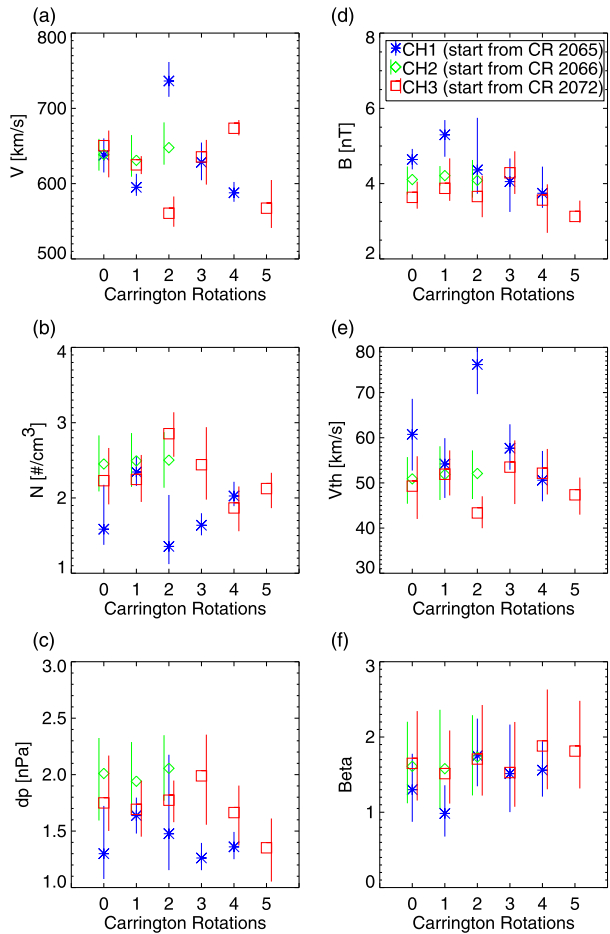


median value of a particular quantity calculated over the whole interval of HSS observations in the course of one CR (see the interval between dashed vertical lines in Figure 2 as an example). The vertical segments show estimates of error bars (the difference between first and third quartiles in our case). Units on the horizontal axis are a number of the CR counted from the beginning of CH observations (i.e., a number of the CR minus start number of the particular CH given in the insert of the top right panel). Although the time of observations is sufficiently long (up to six CRs), we do not observe any systematic change of the median velocity. The median velocity varies in the $520\text{--}730\text{ km s}^{-1}$ range that Heinemann et al. (2018b) associated with the main phase of a CH lifetime. The only parameter suggestive of a systematic evolution is the magnetic field magnitude (Figure 3d). The profile shows a slight increase in the magnetic field in the first two CRs for all three CHs followed by a gradual decrease lasting until the end of observations of each individual CH. Although this trend in the magnetic field is visible and it is supported also by a similar trend in beta parameter (Figure 3f), relatively large uncertainties do not allow us to make any conclusive statement about a temporal trend. Our plots do not reveal any systematic change in the density and thermal speed.

The short-term analysis, i.e. variation within a single HSS, assumes that the spacecraft gradually samples the longitudinal profile of a CH at a fixed latitude in course of one HSS encounter. It means that a temporal profile of each quantity would correspond to its spatial profile at the source region. Since the parameters of all three CHs were similar (Figure 3), we analyze them as one set.

Figure 4 shows a superposed epoch analysis of the magnetic field and plasma parameter profiles for all 14 encounters with HSSs. Since the continuous HSS observations range from 20 to 40 hours, we use the following steps for analysis:

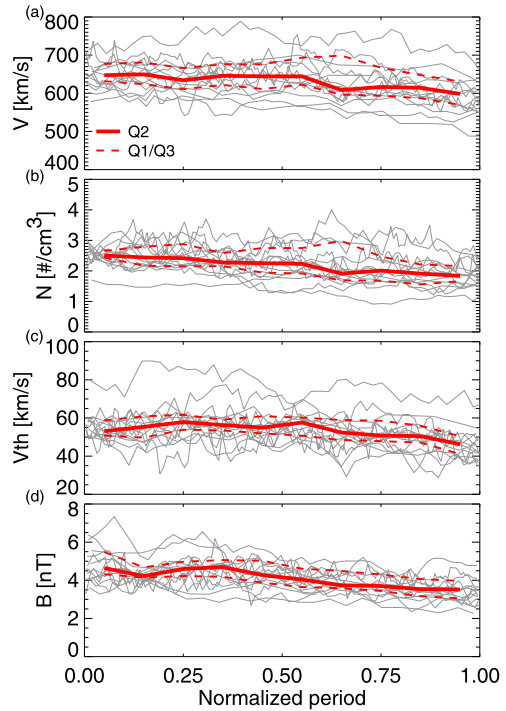
Figure 3 Time evolution of different solar wind parameters for three CHs (CH1-blue, CH2-green, and CH3-red). The units on the horizontal axis are CRs counted from the first observation of a particular CH (identified in panel d’s legend). From top to bottom (left-right): the solar wind speed, IMF magnitude, density, thermal speed, pressure, and plasma beta. The line segments show estimates of error bars determined as the first and third quartiles.



- i) We re-scale the time of HSS observations; 0 corresponds to the leading and 1 to trailing edges of the HSS core.
- ii) We divide each HSS interval into 10 bins and calculated the median values for each bin of individual HSSs.
- iii) We use these medians for a superposed epoch analysis of the median temporal profiles of all HSSs.

Figure 4 shows all individual profiles by the gray lines and the red heavy line stands for median profiles of parameters. The two dashed red lines represent the upper and lower quartiles. The most pronounced feature is a slight gradual decrease of medians of all depicted quantities. However, the longitudinal profiles of parameters at the solar surface do not typically show a decreasing trend in CHs as they rotate from limb to limb. For example, based on the WSA model (Wang et al., 1997), the velocity profile near the Sun should exhibit a peak in the center of the CH and a decrease with a distance from the center. Therefore, any temporal trend in HSSs is unlikely to be the result of longitudinal structure within the CH, but instead the result of the interaction of fast and slow streams. The rarefaction that is typically observed behind the HSS trailing edge is probably observable even within the feature

Figure 4 Superposed epoch analysis of magnetic field and plasma parameters across HSSs as a function of the normalized period. Thin gray lines show individual HSS encounters, the thick red line stands for the medians and dashed red lines represent the first and third quartiles that are given as scatter estimates.



that we have identified as the HSS core (Broiles, Desai, and McComas, 2012; Ďurovcová, Šafráková, and Němeček, 2019).

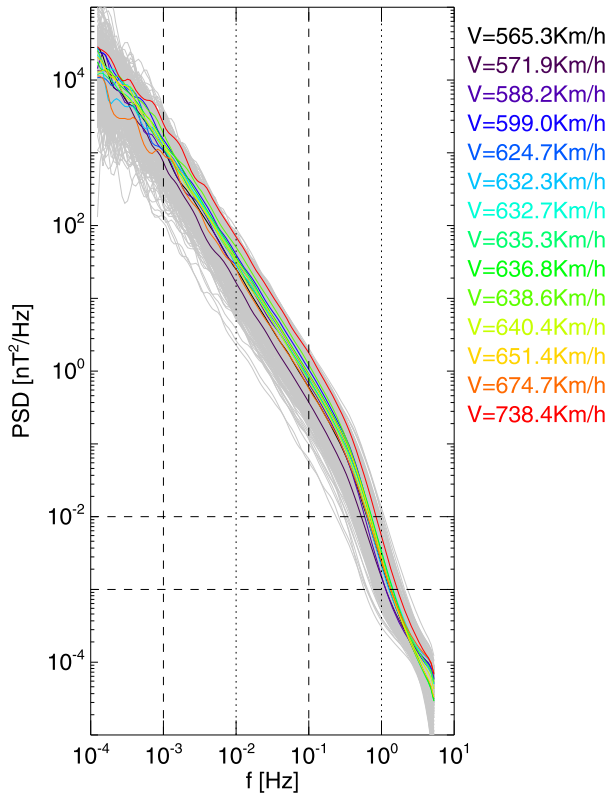
The differences between individual crossings of HSSs could be attributed either to (i) a latitudinal profile of the source region, as consecutive HSS observations provide samples in different latitudes, or to (ii) temporal variations. Since we did not find any clear longitudinal profile of investigated parameters, and this conclusion can be presumably applied also to the latitudinal profile, the interpretation in terms of temporal changes is the most probable. The time span between two consecutive HSS encounters is about one CR.

3.2. Long- and Short-Time Analyses of the Fluctuation Power Within HSSs

PSDs of magnetic field variations were estimated by a continuous wavelet transform (Torrence and Compo, 1998) on each 6.7-hour subinterval (Figure 1). PSDs computed on these subintervals are later used for a presentation of short-term turbulence changes, whereas the averaged PSDs for each HSS encounter serve for a study of long-term variations.

Figure 5 shows the long-term analysis of PSD magnetic field profiles; colored lines represent the average PSD for each individual HSS. No systematic temporal change of the fluctuation power that could be related to the evolution of the source region could be identified. For this reason, colors indicate the median bulk speed within a particular HSS encounter, as solar-wind speed has been previously suggested as a parameter controlling the fluctuation power in the fast wind (e.g. Vasquez et al., 2007). As a comparison with previous results devoted to the analysis of turbulence, the gray lines present PSDs from all periods of the 2008–2009 years when the solar-wind speed was higher than 500 km s^{-1} , no matter whether the interval is related to a CH or not. The criteria for the interval selection were similar to

Figure 5 PSD profiles computed in all intervals of the fast ($V > 500 \text{ km s}^{-1}$) solar wind (gray lines) and in HSSs within CHs (colored lines). The dotted lines denote the frequencies selected as representatives of the power in the MHD (0.01 Hz) and kinetic (1 Hz) ranges and the dashed lines mark the intervals for calculations of the PSD slopes in the MHD (vertical) and kinetic (horizontal) scales.



those applied to HSSs within CHs: (i) a higher solar-wind speed ($> 500 \text{ km s}^{-1}$) for more than 13.5 hours (twice the length of the window we used), and (ii) the compressed parts at leading edges of HSSs were removed. We found 58 intervals under these conditions and we divided them into 381 subintervals. As we noted, we have chosen the power at $f=0.01 \text{ Hz}$ and $f=1 \text{ Hz}$ as representatives of the MHD and kinetic ranges, respectively (frequencies are denoted by the vertical dotted lines in Figure 5).

All PSD profiles of HSSs related to CHs exhibit a similar trend and their powers are limited to small ranges, $1.4 \text{ to } 5.1 \times 10^{-3} \text{ nT}^2/\text{Hz}$ in the kinetic and $15.60 \text{ to } 66.91 \text{ nT}^2/\text{Hz}$ in the MHD range. It is out of our expectation because the fluctuation power in the fast solar wind usually disperses in a wide range as the gray lines confirm (around two orders of magnitude). In spite of our careful selection of fast wind intervals, the spread of all PSDs is much broader than that computed within preselected HSSs from identified CHs.

Since PSDs belonging to our CH intervals are located in the upper part of the gray area, we can conclude that CHs are probably sources of turbulent fluctuations in the fast wind and these fluctuations then dissipate due to an interaction with the surrounding environment (e.g. Borovsky, Denton, and Smith, 2019). Although Figure 5 does not show any clear correlation between the fluctuation power and solar-wind speed, the events with the highest (lowest) solar-wind speeds correspond to the highest (lowest) power in the MHD range. This trend is consistent with Borovsky (2012) but even a brief inspection of Figure 5 would reveal several deviations from this trend. For example, the interval with second highest velocity exhibits the second lowest fluctuation power and other profiles are also not ranked with solar wind speeds clearly.

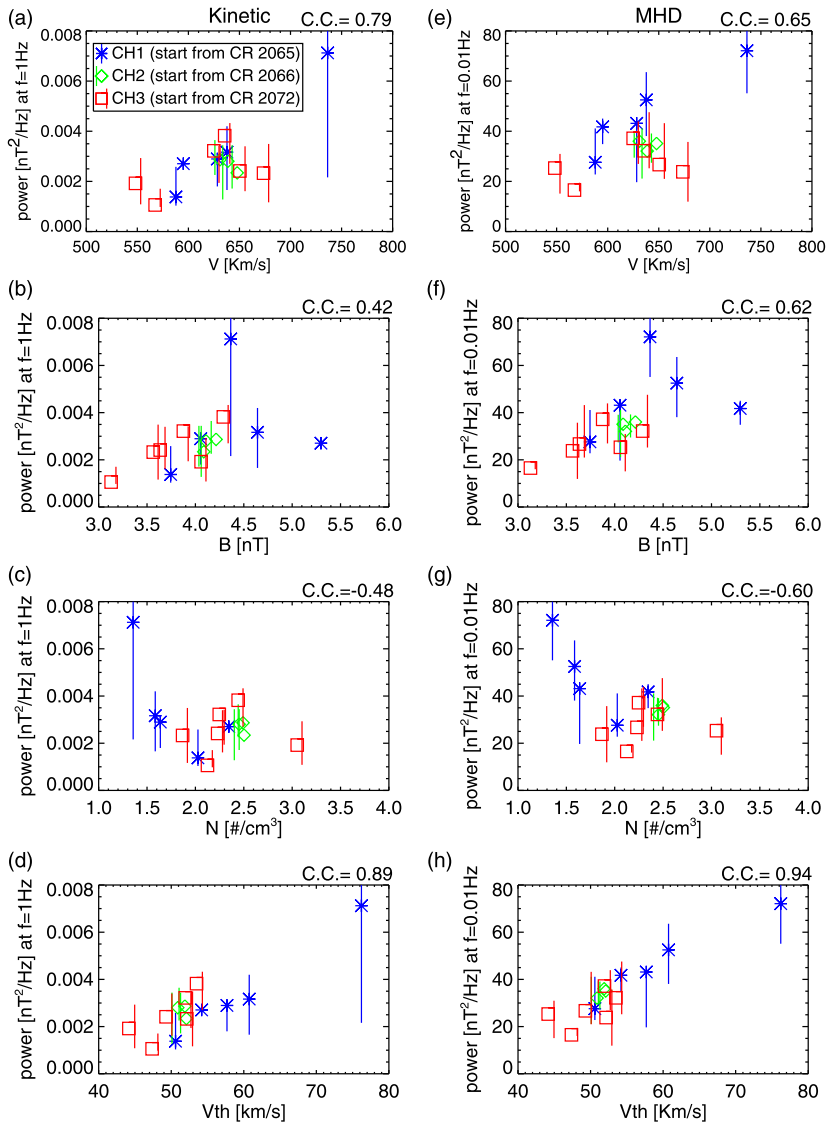


Figure 6 The scatter plots of the average PSD power as a function of the solar wind parameters in the kinetic ($f=1$ Hz; left column) and MHD ($f=0.01$ Hz; right column) ranges. From top to bottom: the bulk speed, magnetic field strength, and density, and thermal speed. The marker colors distinguish the HSS coming from the same CH (CH1-blue, CH2-green, and CH3-red, and denoted in panel a’s legend). Error bars are derived as in Figure 3.

For further understanding of the relationship between the fluctuation power and solar-wind parameters, Figure 6 shows the scatter plots of power as a function of several parameters. Colors and symbols distinguish the HSSs coming from different CHs and the vertical lines represent the differences between first and third quartiles. The left-hand column of panels shows the kinetic scale whereas the MHD scale is shown on the right-hand side. Prior to a discussion of the relation between the fluctuation power and average parameters, we want

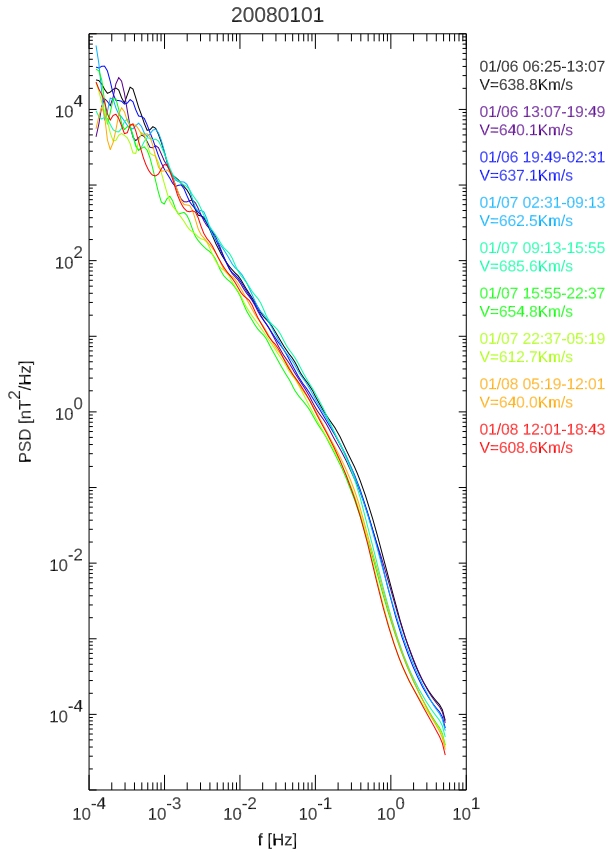
to stress that the power scales are linear and that the smallest and largest powers differ by a factor of five only at both analyzed frequencies. This is contrary to the expectation of large variability in turbulence (around four orders of magnitude) in the fast solar wind (e.g., Smith et al., 2006).

Figure 6a shows a relation between the fluctuation power and solar-wind speed in the kinetic range and we can see that it is an increasing function of the speed with a correlation coefficient of $C.C. = 0.79$ (the P-value is 0.02 when $C.C. = 0.62$). A similar relation can be found also in the MHD range with a $C.C. = 0.65$ (Figure 6e). The relation between the fluctuation power and magnetic field magnitude is not so clear in the two ranges (Figures 6b and 6f). Although the correlation coefficient of 0.62 for the MHD range (Figure 6f) is significant, the correlation in the kinetic range is only 0.42 only. In spite of it, we suggest that the fluctuation power is probably a function of the magnetic field magnitude because the low correlation coefficient may just influence by one outlier. Conversely, Figure 6g shows that the density exhibits a weak negative correlation with the fluctuation power in the MHD range ($C.C. = -0.60$) but the decreasing trend is less clear in the kinetic range. Note that the opposite trends observed for the speed (Figures 6a and 6e) and density (Figures 6c and 6g) are consistent with the anti-correlation of these two parameters, which typical in the fast solar wind. A relation of the thermal speed and fluctuation power is clear in the kinetic range ($C.C. = 0.89$) and even more distinct in the MHD range ($C.C. = 0.94$). Correlation coefficients were calculated for all observations shown in the panels but we stress that similar relations hold for subsets belonging to multiple encounters with the same CH (distinguished by colors and symbols).

As an example of short-term variations of turbulence within a particular HSS, Figure 7 presents PSDs derived from measurements on 2008/01/06–08 (first event in Table 1). This HSS was observed continuously for two and a half days and we divided the observations into nine subintervals (see Figure 1). The colors of profiles correspond to the time of a subinterval inside the HSS, and the median solar-wind speed within each subinterval is given at the right-hand side of the panel. The trends of all profiles are similar and the differences of the fluctuation power among particular profiles are small. A comparison of different colors shows that there is no systematic evolution that could be related to the CH longitudinal profile or a time evolution in the MHD range because, for example, two green curves belong to two consecutive intervals in the middle of the HSS but they are bounding the spread of PSDs in the MHD range. These features are consistent with the results of average PSD profiles for each HSS shown in Figure 5. The power in the kinetic range decreases with time and this feature is also found in short-term evolution of most HSSs, but it is not present in the long-term analysis discussed above.

The relation between the fluctuation power and solar-wind parameters for each subinterval of our example is shown in Figure 8. Similar to Figure 6, the fluctuation power in the MHD range shows a relationship with the solar-wind speed but this dependence vanishes in the kinetic range (compare Figures 8a and 8e; $C.C. = 0.66$ for MHD and $C.C. = 0.22$ for kinetic ranges; the P-value is 0.05 when $C.C. = 0.66$). For the magnetic field, the relations are not so clear (see Figures 8b and 8f) as those for average PSD profiles in Figure 6. The density exhibits a strong positive correlation with the fluctuation power with $C.C. = 0.94$ (Figure 8c) in the kinetic range but not in the MHD range ($C.C. = 0.34$, Figure 8g). These results are slightly different from those shown in Figure 6. The relation between the power of PSDs and the thermal velocity is observed also only in the MHD range, and the correlation coefficient is not as high ($C.C. = 0.71$) as that in Figure 6h ($C.C. = 0.85$). We present only one example from 14 HSS events but most HSSs show a similar behavior. For example, 11 of 14 HSSs exhibit a significant correlation between the solar-wind density and fluctuation power.

Figure 7 The PSD profiles of the subintervals for the HSS event on 2008/01/06–09. The colors correspond to time inside this HSS and average speed is given at the right-hand side of the panel.



3.3. Spectral Indices

The spectral slopes are often considered as important characteristics of turbulence (e.g., Zhou, Matthaeus, and Dmitruk, 2004). We calculated the slopes of PSD profiles by linear fitting in the frequency range of 10^{-1} to 10^{-3} Hz for the MHD range (denoted by the vertical dashed lines in Figure 5) and in the power range from 10^{-2} to 10^{-3} nT²/Hz for the kinetic range (see horizontal dashed lines in Figure 5). Figure 9 presents the distributions of slopes of the PSD profiles calculated for each subinterval (altogether 58 subintervals, black dotted line) and the distributions of PSD slopes averaged for the CH encounters (14 encounters, red solid lines) in the MHD (Figure 9a) and kinetic ranges (Figure 9b). The green and gray regions present histograms for all HSS events without considering the sources. In the MHD range, the values of the slopes averaged for different CH encounters span in a very narrow region between -1.55 to -1.65 . The spread of slopes for individual subintervals is larger (-1.45 – -1.75) but an average value of -1.60 is the same as that for the averaged PSD profiles. In the kinetic range, the slopes of average profiles are significantly steeper and their distribution is much wider with the spread between -3.1 to -3.7 , but the slopes calculated for particular subintervals can exceed -4.0 . These ranges are consistent with the results of previous studies (e.g., Leamon et al., 1998; Smith et al., 2006; Alexandrova et al., 2009; Koval and Szabo, 2013), especially in the MHD range. Nevertheless, a relative small spread of slopes shows that the CH-related HSSs are stable sources of turbulence.

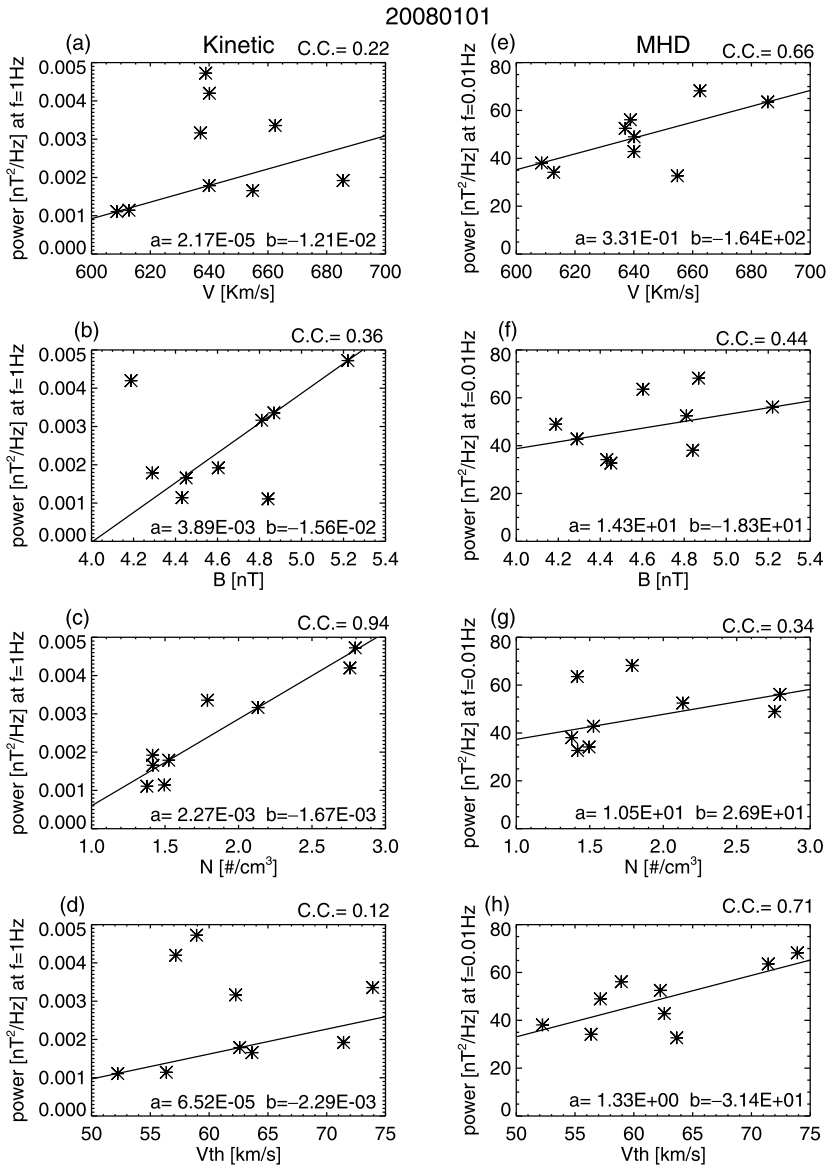


Figure 8 The fluctuation power as a function of solar wind parameters in the kinetic (1 Hz; left column) and MHD (0.01 Hz; right column) ranges. From top to bottom: the scatter plots of the bulk speed, magnetic field strength, density, and thermal speed. Solid lines in the panels are linear fits of data points. Coefficients a and b of the fit equation $y=ax+b$ are given in the panels, the correlation coefficients C.C. can be found above the panel.

4. Discussion

This study investigated magnetic field and plasma parameters observed within HSSs emanating from well identified CHs was to answer two questions: (i) Is there evidence of time evolution of CHs in the spacecraft data? (ii) Is there a typical temporal profile of HSSs that

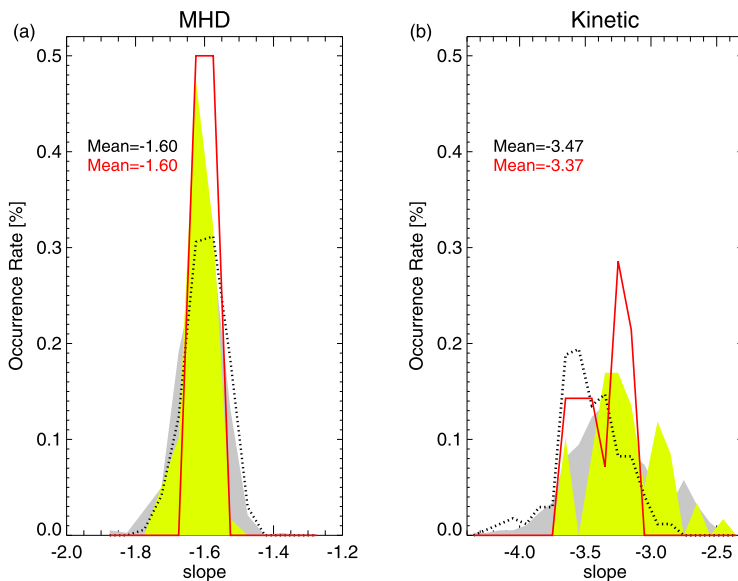


Figure 9 Histograms of the PSD slopes in (a) the MHD and (b) kinetic ranges. The red lines represent the results from averaged PSDs and the black dotted lines present the results of our analysis of the PSDs in each subinterval. Average values are marked in corresponding panels. The green and gray regions illustrate results from all fast wind intervals regardless of the source.

could be related to the longitudinal structure of CHs? The answers are likely negative in both cases. We did not find any reliable evidence of systematic evolution of the solar-wind speed related to the CH age. On the other hand, a gradual evolution of CHs is seen in the magnetic field profiles (Figure 3d). The superposed HSS analysis (Figure 4) revealed a slight gradual rarefaction that probably cannot be connected with a CH longitudinal profile but that develops along the HSS path to the L1 point due to an interaction with the slower ambient wind. We stress that the trailing parts of HSSs were excluded from our analysis (see Figure 2). However, most solar-wind parameters decreased with time, especially the density, thus we suggest that the rarefaction is observable even within the HSS core. The rarefaction is typically accompanied by the plasma cooling in the region following the HSS core but the median profile of the thermal speed (Figure 4) exhibits a weak enhancement in the HSS center. This enhancement probably reflects a longitudinal profile of the source region because it is visible only when the general decreasing trend is taken into account.

Since the observed rarefaction would be a result of the HSS interaction with the slower ambient wind, we suggest that this interaction excites waves that propagate into the HSS core. The second issue considered in this study is the long- and short-term evolution of magnetic field fluctuations within HSSs related to CHs. To characterize these fluctuations, we have divided each HSS observation into 6.7-hour subintervals and computed the PSD on these subintervals. A comparison of PSDs from one HSS observation served for a discussion of the short-term variations, whereas the long-term changes were studied over multiple solar rotations using the medians of PSDs for each HSS encounter. In order to put our results into the context of previous work, we also selected sufficiently long (14 hours or more) continuous observations of the fast ($> 500 \text{ km s}^{-1}$) solar wind for the year 2008 and processed in the same manner. Turbulence within HSSs was studied by Bruno et al. (2017) that compared different parts of stream interaction regions but our study focuses on the HSS core only.

Table 2 The slopes and powers of the HSSs in kinetic and MHD ranges.

		Kinetic			MHD		
		Maximum	Median	Minimum	Maximum	Median	Minimum
All HSS	Slope	-2.46	-3.21	-4.35	-1.39	-1.61	-1.87
	Power	0.0061	0.0021	0.0007	87.08	23.61	2.81
CH-related HSS	Slope	-3.14	-3.48	-3.64	-1.57	-1.59	-1.63
	Power	0.0051	0.0026	0.0014	66.91	32.34	15.60

Results of our study are summarized in Table 2. We found that the HSSs originating from CHs are very stable sources of turbulence because the power in both MHD and kinetic ranges varies within a factor of 5, whereas more than an order of magnitude variations were found in the fast wind in general. The same trend is found for the spectral indices of PSDs. Although median values are ~ -1.6 in the MHD range regardless of the fast wind origin, the slopes of PSDs vary over a much narrower range for HSSs related to CHs. In the kinetic range slopes lie between -2.46 and -4.35 for the fast wind in general and between -3.14 and -3.64 for HSSs related to CHs. Recent studies indicate slopes of about -2.8 in the kinetic range (e.g., Alexandrova et al., 2009, 2012; Sahraoui et al., 2013; Chen et al., 2013; Koval and Szabo, 2013), shallower than those reported in this study. However, Smith et al. (2006) found that the PSDs of open and cloud-like IMF structures have different slopes. The slopes for the open IMF are much steeper and our HSSs are clearly on open solar flux. Moreover, slopes of -2.8 often result from the PSD profile of perpendicular fluctuations, but we use the sum of all three components to account for both perpendicular and compressible fluctuations.

As with the averages of the magnetic field and plasma parameters, our study does not indicate any systematic evolution of the power and spectral properties of magnetic field fluctuations in CHs over multiple solar rotations. We found that the fluctuation power correlates with the bulk and thermal velocities and anti-correlates with the density in both MHD frequency ranges (Figure 6g). Borovsky (2012) reported the correlation between the power of magnetic field magnitude fluctuations and the bulk solar-wind speed with $C.C. = 0.68$. This result reflects a behavior of a compressible component that is minor in the fast wind (e.g., Šafránková et al., 2019). Our study shows that this relation holds also for the perpendicular fluctuations. It is known that the density exhibits an anti-correlation with the solar-wind speed and thus the density shows an anti-correlation with the fluctuation power in both frequency ranges. The relations between the thermal speed and fluctuation power can be explained in two ways: the higher turbulence power provides more energy to heat the plasma, or the hot plasma environment is favorable for excitation of waves and fluctuations.

The solar wind observed at different times through a single HSS emanates from the footprints at different longitudes in the CH, and is therefore a mix of temporal and spatial variability. Our study of long-term variations has shown that CHs are stable structures that usually exist for several solar rotations and thus their properties cannot quickly change within a few days. Consequently, we may assume that short-term variations are mainly influenced by the spatial effects. The PSDs calculated for each subinterval in individual HSS events show that fluctuation power decreases with time in the kinetic range (Figure 7). However, such a feature was not found in the long-term evolution and thus it cannot be a clue to the temporal evolution. Since the solar wind observed at different times within the HSS crossing emanates from different parts of the CH, this inconsistency implies that turbulence

has probably slightly different properties in different source regions within the particular CH. This interpretation is supported by the fact that temporal variations of the fluctuation power in the inertial range are not regular in all the HSSs.

As we already noted, the density within a HSS usually exhibits a decreasing trend with time (Figure 4). We argue that this trend is not formed in the source region but it is probably related to compression/rarefaction effects in the CIR. The density profile within a main body of the HSS would be formed by compressional waves propagating from the stream interface into this region. Therefore, the relation between the density and fluctuation power can be probably attributed to additional compressional waves generated in the CIR region. This interpretation is supported by the fact that the density (Figure 8) correlates with the fluctuation power in the kinetic range and the fluctuations in this range of frequencies are more compressive (Šafránková et al., 2019). On the other hand, a typical relation between the velocity and fluctuation power in the MHD range is not observed (compare panels 8a and 8c). The other possible reason for a positive correlation between the density and fluctuation power is the spatial structure of the source regions. It is known that there are different substructures like bright points in CHs (e.g., Huang et al., 2012) and thus we cannot exclude that the relation between the density and fluctuation power originates in source regions.

5. Summary and Conclusions

The study is based on an analysis of cores of 14 HSSs emanating from three equatorial CHs observed at L1. We excluded compressed regions at HSS leading edges as well as rarefaction regions following their trailing edges. These two regions are (i) strongly affected by the HSS interaction with the slower ambient solar wind and (ii) map onto a very narrow region at the CH boundary. On the other hand, a temporal profile of the HSS core would provide information on the longitudinal profile of its source. A comparison of consecutive observations of the same CH reflects its temporal evolution on a scale of CRs.

An analysis of averaged parameters revealed that:

(i) For velocity and other plasma quantities within HSSs no systematic changes from one to following HSS encounter are observed. The three-stage evolution of CH life cycle (Heinemann et al., 2018b) can be identified in the magnetic field magnitude only.

(ii) Temporal profiles of the averaged magnetic field and plasma density and velocity across the HSS are flat; a slight gradual decrease can be probably attributed to the HSS interaction with the slower ambient wind.

(iii) The temperature peaks at the middle of a CH but an excess above the general decreasing trend is about 10–15% only.

The PSD spectra typically have a power-law form, but the power and slopes vary under different solar-wind conditions. Differences between consecutive encounters of the HSS emitted from the same CH are caused partly by the temporal evolution of a HSS on a time scale of solar rotations and partly by the latitudinal structure of the CH. On the other hand, short-term variations of the fluctuation power and PSD slopes within one HSS were attributed to the HSS evolution on its transit from the Sun to near-Earth space. A strong correlation between the fluctuation level and solar-wind density in the kinetic range (Figure 8c) is probably a result of compressional waves propagating into the main part of HSSs.

We emphasize that all average PSD profiles computed within HSSs exhibit similar trends and the fluctuation power is limited to a small range. Since CHs under study are widely separated in time and in longitudes, we propose that these results can be generalized to all CHs. Finally, we can conclude that:

(i) CHs are very stable sources of turbulent fluctuations; their spectral properties (power and spectral slopes in MHD and kinetic ranges) vary in very narrow ranges in a comparison with the fast wind period regardless of the sources.

(ii) The average slopes are -1.60 ± 0.02 for the MHD and -3.37 ± 0.18 for kinetic ranges.

(iii) The large variability of PSDs reported for the fast wind (e.g. Smith et al., 2006) does not originate in CHs; it reflects properties of other fast solar-wind sources or it is a result of the interaction with the surrounding slow solar wind.

Acknowledgements The authors acknowledge the Wind team for data use via <http://cdaweb.gsfc.nasa.gov/cdaweb/>. The present work was supported by the Czech Science Foundation under Contract 19-18993S and by the Ministry of Science and Technology in Taiwan under grant MOST-108-2111-M-008-019.

Disclosure of Potential Conflict of Interest We declare we have no conflicts of interest.

Publisher's Note Springer Nature remains neutral with regard to jurisdictional claims in published maps and institutional affiliations.

References

- Alexandrova, O.: 2008, Solar wind vs magnetosheath turbulence and Alfvén vortices. *Nonlinear Process. Geophys.* **15**, 95. DOI.
- Alexandrova, O., Saur, J., Lacombe, C., Mangeney, A., Mitchell, J., Schwartz, S.J., Robert, P.: 2009, Universality of solar-wind turbulent spectrum from MHD to electron scales. *Phys. Rev. Lett.* **103**(16), 165003. DOI.
- Alexandrova, O., Lacombe, C., Mangeney, A., Grappin, R., Maksimovic, M.: 2012, Solar wind turbulent spectrum at plasma kinetic scales. *Astrophys. J.* **760**(2), 121. DOI.
- Borovsky, J.E.: 2012, The velocity and magnetic field fluctuations of the solar wind at 1 AU: Statistical analysis of Fourier spectra and correlations with plasma properties. *J. Geophys. Res.* **117**, A05104. DOI.
- Borovsky, J.E., Denton, M.H., Smith, S.W.: 2019, Some properties of the solar wind turbulence at 1 AU statistically examined in the different types of solar wind plasma. *J. Geophys. Res.* **124**, 4. DOI.
- Broiles, T.W., Desai, M.I., McComas, D.J.: 2012, Formation, shape, and evolution of magnetic structures in CIRs at 1 AU. *J. Geophys. Res.* **117**, A3. DOI.
- Bruno, R., Carbone, V.: 2013, The solar wind as a turbulence laboratory. *Living Rev. Solar Phys.* **10**, 2. DOI.
- Bruno, R., Telloni, D.: 2015, Spectral analysis of magnetic fluctuations at proton scales from fast to slow solar wind. *Astrophys. J.* **2**, L17. DOI.
- Bruno, R., Trenchi, L., Telloni, D.: 2014, Spectral slope variation at proton scales from fast to slow solar wind. *Astrophys. J. Lett.* **793**, L15. DOI.
- Bruno, R., Telloni, D., DeLure, D., Pietropaolo, E.: 2017, Solar wind magnetic field background spectrum from fluid to kinetic scales. *Mon. Not. Roy. Astron. Soc.* **472**, 1052. DOI.
- Chen, C.H.K., Boldyreov, S., Xia, Q., Perez, J.C.: 2013, Nature of subproton scale turbulence in the solar wind. *Phys. Rev. Lett.* **110**, 225002. DOI.
- Đurovcová, T., Šafráková, J., Němeček, Z.: 2019, Evolution of relative drifts in the expanding solar wind: Helios observations. *Solar Phys.* **294**, 7. DOI.
- Gallagher, P.T., Moon, Y.J., Wang, H.: 2020, Active-region monitoring and flare forecasting – I. Data processing and first results. *Solar Phys.* **209**, 171. DOI.
- Heinemann, S.G., Temmer, M., Hofmeister, S.J., Veronig, A.M., Vennerstrøm, S.: 2018a, Three-phase evolution of a coronal hole. I. 360° remote sensing and in situ observations. *Astrophys. J.* **861**, 151. DOI.
- Heinemann, S.G., Hofmeister, S.J., Veronig, A.M., Temmer, M.: 2018b, Three-phase evolution of a coronal hole, Part II: The magnetic field. *Astrophys. J.* **863**, 29. DOI.
- Huang, Z., Madjarska, M., Doyle, G., Lamb, D.: 2012, Evolution of magnetic field corresponding to X-ray brightening events in coronal holes and quiet Sun. *Proc. Int. Astron. Union* **8**(S294), 155. DOI.
- Kasper, J.C., Lazarus, A.J., Steinberg, J.T., Ogilvie, K.W., Szabo, A.: 2006, Physics-based tests to identify the accuracy of solar wind ion measurements: A case study with the wind Faraday cups. *J. Geophys. Res.* **111**, A03105. DOI.

- Kiyani, K.H., Osman, K.T., Chapman, S.C.: 2015, Dissipation and heating in solar wind turbulence: From the macro to the micro and back again. *Phil. Trans. Roy. Soc. A* **373**, 20140155. DOI.
- Kiyani, K.H., Chapman, S.C., Sahraoui, F., Hnat, B., Fauvarque, O., Khotyaintsev, Y.V.: 2013, Enhanced magnetic compressibility and isotropic scale invariance at sub-ion Larmor scales in solar wind turbulence. *Astrophys. J.* **763**, 10. DOI.
- Koval, A., Szabo, A.: 2013, Magnetic field turbulence spectra observed by the wind spacecraft. *AIP Conf. Proc.* **1539**, 211. DOI.
- Krista, L.D., Gallagher, P.T.: 2009, Automated coronal hole detection using local intensity thresholding techniques. *Solar Phys.* **256**(1–2), 87. DOI.
- Leamon, J., Smith, C.W., Ness, N.F., Mattaeus, W.H., Wong, H.K.: 1998, Observational constraints on the dynamics of the interplanetary magnetic field dissipation range. *J. Geophys. Res.* **103**, A3. DOI.
- Lepping, R.P., Acuña, M.H., Burlaga, L.F., Farrall, W.M., Slavin, J.A., Schatten, K.H., et al.: 1995, The WIND magnetic field investigation. *Space Sci. Rev.* **71**, 207. DOI.
- Matteini, L., Horbury, T.S., Neugebauer, M., et al.: 2014, Dependence of solar wind speed on the local magnetic field orientation: Role of Alfvénic fluctuations. *Geophys. Res. Lett.* **41**(2), 259. DOI.
- Ogilvie, K.W., Chornay, D.J., Fritzenreiter, R.J., et al.: 1995, SWE, a comprehensive plasma instrument for the wind spacecraft. *Space Sci. Rev.* **71**(1–4), 55. DOI.
- Pitňa, A., Šafránková, J., Němeček, Z., Franci, L., Pi, G., Montagud, C.V.: 2019, Characteristics of solar wind fluctuations at and below ion scales. *Astrophys. J.* **879**, 82. DOI.
- Šafránková, J., Němeček, Z., Němec, F., Verscharen, D., Chen, C.H.K., Ďurovcová, T., Riazantseva, M.O.: 2019, Scale-dependent polarization of solar wind velocity fluctuations at the inertial and kinetic scales. *Astrophys. J.* **870**(1), 40. DOI.
- Sahraoui, F., Goldstein, M.L., Belmont, G., Canu, P., Rezeau, L.: 2010, Three dimensional anisotropic K spectra of turbulence at subproton scales in the solar wind. *Phys. Rev. Lett.* **105**, 131101. DOI.
- Sahraoui, F., Huang, S.Y., Belmont, G., Goldstein, M.L., Retinò, A., Robert, P., De Patoul, J.: 2013, Scaling of the electron dissipation range of solar wind turbulence. *Astrophys. J. Lett.* **777**, 15. DOI.
- Smith, C.W., Hamilton, K., Vasquez, B.J., Leamon, R.J.: 2006, Dependence of the dissipation range spectrum of interplanetary magnetic fluctuations on the rate of energy cascade. *Astrophys. J. Lett.* **645**, L85. DOI.
- Torrence, C., Compo, G.P.: 1998, A practical guide to wavelet analysis. *Bull. Am. Meteorol. Soc.* **79**(1), 61. DOI.
- Vasquez, B.J., Smith, C.W., Hamilton, K., MacBride, B.T., Leamon, R.J.: 2007, Evaluation of the turbulent energy cascade rates from the upper inertial range in the solar wind at 1 AU. *J. Geophys. Res.* **112**, A7. DOI.
- Wang, Y.-M., Sheeley, N.R., Phillips, J.L., Goldstein, B.E.: 1997, Solar wind stream interactions and the wind speed-expansion factor relationship. *Astrophys. J.* **488**, L51. DOI.
- Zhao, L., Zurbuchen, T.H., Fisk, L.A.: 2009, Global distribution of the solar wind during solar cycle 23: ACE observations. *Geophys. Res. Lett.* **36**, L14104. DOI.
- Zhou, Y., Matthaeus, W.H., Dmitruk, P.: 2004, Colloquium: Magnetohydrodynamic turbulence and time scales in astrophysical and space plasmas. *Rev. Mod. Phys.* **76**, 1015. DOI.